J. Mol. Biol. (1985) **182**, 131–149

Structure and Polymorphism of Bipolar Isopranyl Ether Lipids from Archaebacteria

Annette Gulik, Vittorio Luzzati

Centre de Génétique Moléculaire
C.N.R.S., Gif-sur-Yvette, 91190, France

Mario De Rosa and Agata Gambacorta

Istituto di Chimica di Molecole di Interesse Biologico
C.N.R., Via Toiano 6, Arco Felice, Napoli, Italy

(Received 14 September 1984)

We describe in this work the structure and polymorphism of a variety of lipids extracted from *Sulfolobus solfataricus*, an extreme thermoacidophilic archaebacterium growing at about 85°C and pH 2. These lipids are quite different from the usual fatty acid lipids of eukaryotes and prokaryotes: each molecule consists of two C_{40} ω–ω' biphytanyl residues (with 0 to 4 cyclopentane groups per residue), ether linked at both ends to two (variably substituted) glycerol or nonitol groups. Four lipid preparations were studied; the total and the polar lipid extracts, and two hydrolytic fractions, the symmetric glycerol dialkyl glycerol tetraether and the asymmetric glycerol dialkyl nonitol tetraether, as a function of water content and temperature, using X-ray scattering techniques. The main conclusions from the study of the four lipid preparations can be summarized as follows. (1) As with other lipids, a remarkable number and variety of phases are observed over a temperature–concentration range close to "physiological" conditions. The possibility is discussed that this polymorphism reflects a fundamental property of lipids, closely related to their physiological rôle. (2) As in other lipids, two types of chain conformations are observed: a disordered one (type α) at high temperature; at lower temperature, a more ordered packing of stiff chains, all parallel to each other (type β'). At temperatures and degrees of hydration approaching the conditions prevailing in the living cell, the conformation is of type α. (3) In all the phases with chains in the α conformation, the unsubstituted glycerol headgroups, whose concentration is high in these lipids, segregate in the hydrocarbon matrix, away from the other polar groups. This property may have interesting biological consequences: for example, the chains of a fraction of the bipolar lipid molecules can span hydrocarbon gaps as wide as 75 Å. (4) Two cubic phases are observed in the total and the polar lipid extracts, which display a remarkable degree of metastability, most unusual in lipid phase transitions involving structures with chains in the α conformation. This phenomenon can be explained by the interplay of the physical structure of the cubic phases (the two contain two intertwined and unconnected three-dimensional networks of rods) and the chemical structure of the lipid molecules: the two headgroups of most molecules being anchored on each of the two networks of rods, the migration of the lipid molecules is hindered by the two independent diffusion processes and by the entanglement of the chains. The possibility is discussed that this phenomenon may reflect an evolutionary response to a challenge of the natural habitat of these archaebacteria.

1. Introduction

In the last few years archaebacteria, a novel class of micro-organisms, have been the object of intense studies and of exciting speculations. These organisms are commonly encountered in exceptional ecological niches: methanogens in the absence of oxygen and in the presence of hydrogen and carbon dioxide, halophiles at high salt concentration (i.e. saturated brines), thermoacidophiles at high temperature and acidic pH (90°C and pH 2 are not unusual). A variety of phylogenetic arguments has led some authors to propose archaebacteria as a

0022-2836/85/050131-19 $03.00/0

third primary kingdom of living organisms, the two others being prokaryotes and eukaryotes, and to suggest that archaebacteria may have played a key rôle in the early history of life (for a review, see Woese, 1981).

From a chemical viewpoint, much is known about the structure of the molecular components of archaebacteria (see Kandler, 1982). We are concerned in this work with the lipids, whose chemical structure is remarkably different from that of other organisms (De Rosa *et al.*, 1982, 1983*a,b,c*; Langworthy, 1977, 1982; Comita & Gagosian, 1983). As sketched in Figure 1, the lipid molecules of eukaryotes and prokaryotes consist predominantly (though not uniquely) of two linear hydrocarbon chains of variable length and degree of saturation, ester linked to a glycerol group whose third hydroxyl is substituted by a polar residue. In archaebacteria, some or all of the lipid molecules contain branched hydrocarbon chains of the phytanyl type, ether linked to a substituted or unsubstituted glycerol. *Sulfolobus solfataricus*, whose lipids we have studied in this work, presents the extreme situation of the lipid molecules all

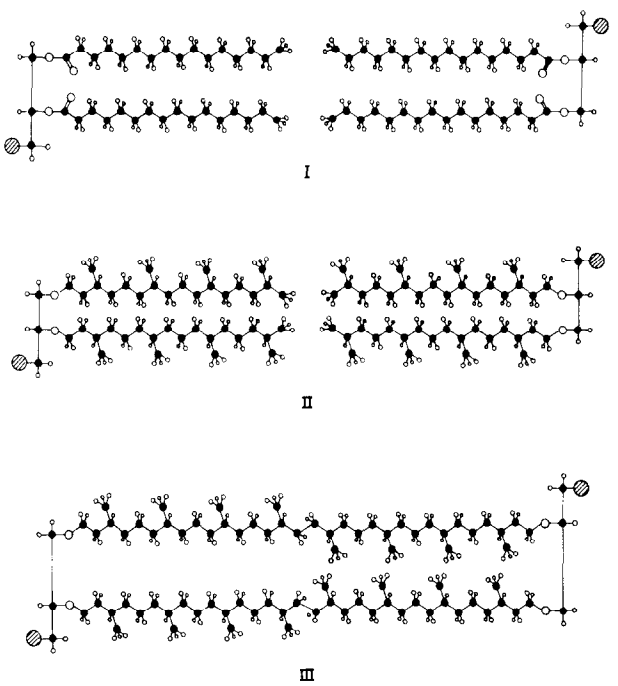

Figure 1. Three examples of lipid molecules, apposed as in lipid bilayers. Filled circles, carbon atoms; open circles, oxygen atoms; small circles, hydrogen atoms; hatched circles, polar residues. I, lipid of eukaryotes and prokaryotes; the hydrocarbon chains are linear (palmitate in this case) and ester linked to glycerol. II and III, lipids of archaebacteria; the hydrocarbon chains are branched (isopranyl) and ether linked to glycerol. Each molecule of type II contains 2 C_{20} chains linked to 1 glycerol; lipids of this type are commonly found in halophiles and in methanogens. III is a dimer of II; it consists of 2 C_{40} chains ether linked at both ends to glycerol groups. The lipids of *S. solfataricus* studied in this work belong to type III, with 0 to 4 cyclopentane groups along each of the isopranyl chains (see Fig. 2).

consisting of two C_{40} ω–ω' biphytanyl residues, with 0 to 4 cyclopentane groups per chain, ether linked at both ends to glycerol or nonitol groups (see Fig. 1: see also De Rosa *et al.*, 1977, 1980*a*, 1983*c*).

Presumably, notwithstanding the differences in growth conditions, the membranes of archaebacteria, prokaryotes and eukaryotes all carry out similar physiological functions. The question may thus be asked how so widely different lipid molecules manage to perform the same functions and why is that variability required for life. These questions bear on the more general problem of the physiological rôle of lipids. According to a widespread opinion, most vividly expressed in the bilayer model, lipids are passive components and only proteins are considered as functional elements of membranes. Without denying the obvious importance of proteins, a few authors have put forward the view that lipids may well play a more subtle structural rôle. The ground for this hypothesis is the remarkable polymorphism of lipids: no other class of biological compounds is known to display such a large number of such a wide variety of structures over such a narrow range of parameters (temperature, water content, chemical composition), and so near to physiological conditions (for reviews, see Luzzati, 1968; Shipley, 1973; Luzzati & Tardieu, 1974). The biological relevance of these polymorphic transitions has been discussed in terms of spatial and temporal fluctuations of the structure of the lipid matrix possibly being involved in some physiological events (Luzzati & Husson, 1962; Luzzati *et al.*, 1966; Luzzati, 1968). This hypothesis has been with us for quite some time but, in spite of a recent revival (de Kruijff *et al.*, 1984) it has not yet received unequivocal experimental support; nor, indeed, rebuttal (Luzzati, 1981). This work is an extension of previous studies of lipid polymorphism, prompted by the hope that such odd members of the lipid family could provide some fresh answer to old questions.

In this work, we have studied four lipid preparations from *S. solfataricus*: total and polar lipid extracts, and two hydrolytic fractions. We have explored the temperature–concentration-dependent phase diagrams of the lipid–water systems, identified the phases and determined their structure, using mainly X-ray scattering techniques.

2. Materials and Methods

The micro-organism *S. solfataricus*, strain MT-4, was grown at 87°C, pH 3·5, as described by De Rosa *et al.* (1975). The total lipids were extracted with chloroform/methanol (1 : 1, v/v); extraction of TLE† with *n*-hexane yielded the polar lipid extract. TLE was also hydrolysed

† Abbreviations used: TLE and PLE, total and polar lipid extract; GDGT, glycerol dialkyl glycerol tetraether; GDNT, glycerol dialkyl nonitol tetraether; e.s.r., electron spin resonance.

with methanolic HCl for 6 h under reflux, and the hydrolytic mixture chromatographed on silica gel columns. Two lipid species were eluted: the symmetric glycerol dialkyl glycerol tetraether, and the asymmetric glycerol dialkyl nonitol tetraether (De Rosa *et al.*, 1983*c*).

The X-ray scattering experiments were performed *in vacuo* on a temperature-controlled Guinier camera using CuKα_1 radiation (λ = 1·54 Å). The samples, prepared by mixing controlled amounts of lipid and water, were sealed in vacuum-tight holders between thin mica windows and studied as a function of temperature. Positions in reciprocal space are specified by the parameter $s = 2 \sin \theta/\lambda$, where 2θ is the scattering angle and λ is the wavelength. The intensities of the reflections were determined by integration of the microdensitometer tracings (Joyce–Loebl, type MKIIICS) and multiplication by s^2.

We refer below to 2 distinct regions of the X-ray scattering spectra: one at low ($s < 0{\cdot}15$ Å^{-1}), the other at high angles ($s > 0{\cdot}15$ Å^{-1}). This is a convenient operational separation, since the small-angle signals arise from the long-range organization of the lipid molecules, whereas the high-angle information reflects the short-range conformation of the hydrocarbon chains.

The phase diagrams were explored by performing X-ray scattering experiments as a function of water content and temperature. Unless otherwise stated, the observations reported below are all considered to be at thermodynamic equilibrium, on the ground that the experimental results are independent of, or barely dependent upon, the previous history of the sample. It is worth noting that the exposure times are of the order of hours in the case of GDNT, TLE and PLE, of days in the case of GDGT (see below). As a rule, if over a finite region of the phase diagram only one type of lattice is observed, and if the lattice parameters and the intensities of the reflections are found to vary continuously, then that region is presumed to contain only one phase. It must be pointed out, however, that the diffuse scattering signals produced by poorly ordered phases may well pass unnoticed in the presence of the sharp reflections due to well-ordered phases.

The first step in the structure analysis of each phase is to identify its X-ray scattering diagram. The second step is to specify the nature of the structure elements (for example, the polar and the hydrocarbon moieties) and to evaluate their volume; volumes are determined easily when the number of electrons and the electron density are known. If, moreover, a shape is ascribed to the structure elements, then their dimensions can be determined also. The final step is the analysis of the intensity of the reflections in terms of the electron density distribution.

The lipids used in this work are remarkably stable: chromatographic analyses carried out on samples that had undergone the harshest treatments involved in the X-ray scattering study failed to detect any chemical alteration.

3. Results

(a) *Chemical composition*

All the lipid molecules, with the exception of a small amount of neutral lipids (see below), contain two biphytanyl chains ether linked at both ends to either a glycerol or a nonitol group; the free OH group of glycerol and one of nonitol may be substituted by a variety of polar groups (De Rosa *et al.*, 1980*b*). Each biphytanyl chain contains 0 to 4 pentane cycles (Fig. 2); the number and position of the cycles depend on the nature of the lipids and vary with the temperature of growth, much like length and degree of unsaturation in prokaryote and eukaryote lipids (De Rosa *et al.*, 1980*c*). Typically, the lipids used in this work contain an average of 2·3 cyclopentane groups per chain.

All of the lipid molecules are derived from two compounds:

I. Glycerol dialkyl glycerol tetraether

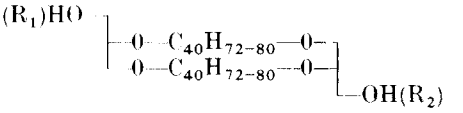

II. Glycerol dialkyl nonitol tetraether

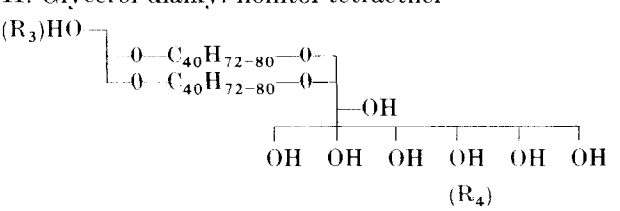

(—$C_{40}H_{72-80}$—) represents the biphytanyl chains (see Fig. 2). In the molecules of the total and the polar lipid extracts, some of the hydroxyl hydrogen atoms are substituted by the polar groups R_1 to R_4 (see below, and De Rosa *et al.*, 1983*a*).

The total lipid extract has the following (weight) composition (De Rosa *et al.*, 1980*b*):

4·5% glycolipids, derived from GDGT with R_1 = H, R_2 = β-D-galactopyranosyl-β-D-galactopyranose ($\bar{M}_r$ 1614);

10·5% glycolipids, derived from GDNT with R_3 = H, R_4 = β-D-glucopyranosyl ($\bar{M}_r$ 1632);

6·0% phospholipids, derived from GDGT with R_1 = H, R_2 = phosphomyoinositol ($\bar{M}_r$ 1532);

8·0% sulpholipids, derived from GDNT with R_3 = H, R_4 = β-D-glucopyranosyl sulphate ($\bar{M}_r$ 1712);

6·0% phospholipids, derived from GDGT with R_1 = β-D-galactopyranosyl-β-D-glucopyranoside, R_2 = phosphoinositol ($\bar{M}_r$ 1856);

42·0% phospholipids, derived from GDNT with R_3 = phosphomyoinositol, R_4 = β-D-glucopyranosyl ($\bar{M}_r$ 1874);

16·0% neutral lipids (mainly hydrocarbons, benzo [b] thiophen-4,7-quinone and a mixture of partially and fully reduced glycerol tri(geranyl geranyl) triethers (see also Tornabene *et al.*, 1979).

The volumes and number of electrons adopted in this work are given in Table 1. For reasons that will be made clear below, it is convenient to divide each lipid molecule into three parts.

In the case of the hydrated phases, it is useful to introduce a parameter specifying the volume concentration of the polar moiety, containing the polar groups of the molecules and water:

$$c_{v,\,pol} = \frac{n_{lip} + c_e(\rho_{H_2O} v_{pol} - n_{lip})}{n_{lip} + c_e(\rho_{H_2O} v_{lip} - n_{lip})}. \qquad (1)$$

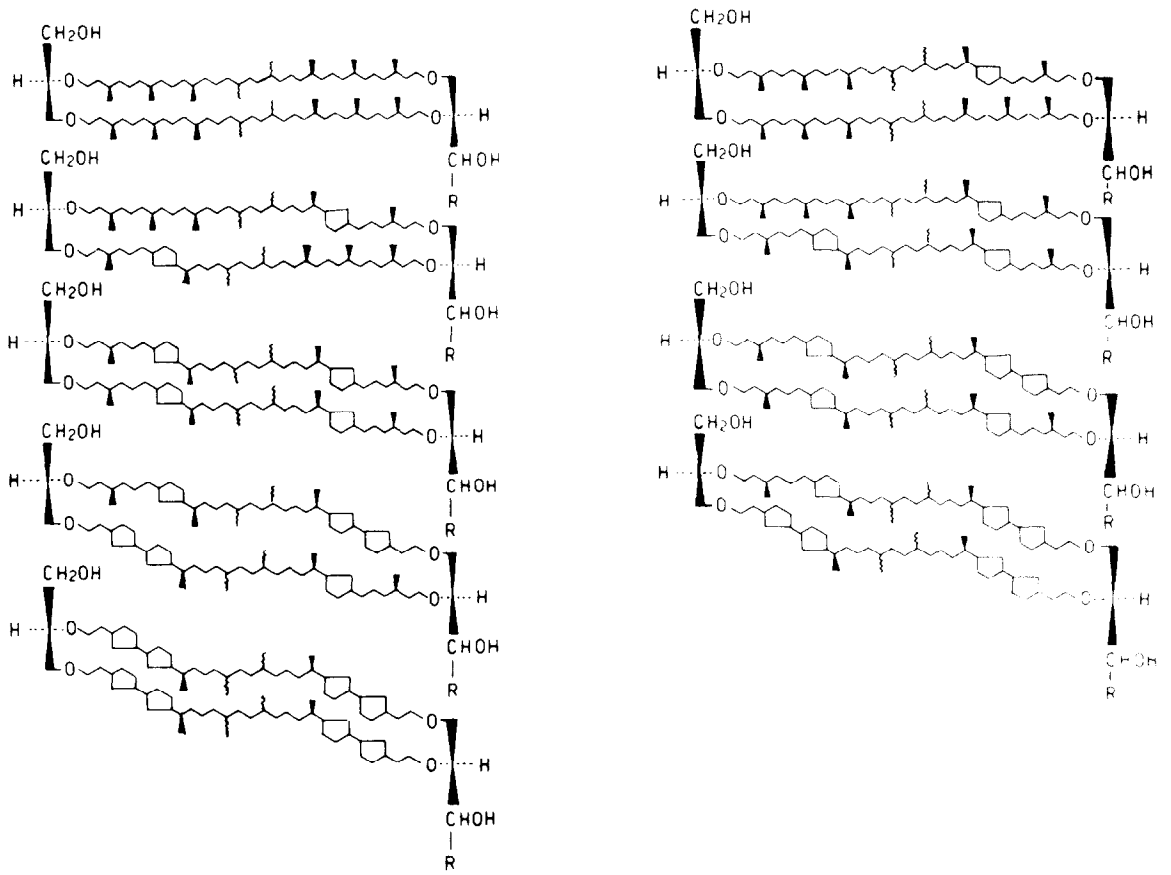

Figure 2. Structure of bipolar isopranyl ethers, the backbone of the complex lipids of *S. solfataricus*. R = H in glycerol dialkyl glycerol tetraether (GDGT):

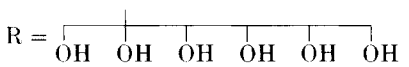

in glycerol dialkyl nonitol tetraether (GDNT). Black arrows and wriggles mean, respectively, known and unknown chirality (from De Rosa *et al.*, 1983*c*).

where c_e is the electron concentration (number of electrons of lipid per number of electrons of the sample), ρ_{H_2O} is the electron density of water (0·334 e Å^{-3} at 20°C), n_{lip} and v_{lip} are the number of electrons and the volume of the average lipid molecule, v_{pol} is the volume of the polar head (see Table 1). Similarly, the expression of the volume concentration of the paraffin moiety is:

$$c_{v,par} = 1 - c_{v,pol}. \qquad (2)$$

(b) *Glycerol dialkyl glycerol tetraether*

Two samples were studied as a function of temperature: one in the absence of added water, the other in the presence of excess water. As a consequence of the low electron density contrast (see Table 1), the small-angle X-ray scattering signals are very weak in this case.

In the absence of water, a lamellar phase is observed at low temperature, characterized by a set of sharp small-angle reflections of spacings a, $a/2$, $a/3$, etc. and by a high-angle band with a clearcut inner edge at $s = 0{\cdot}198$ Å^{-1} (Fig. 3, curve A), modulated by several weak and sharp signals (not visible in the Fig.). The repeat distance $a = 35{\cdot}9$ Å is independent of temperature (within 0·5%) in the range −19 to +19°C. In the vicinity of 19°C, the sharp small-angle and high-angle reflections give way to two diffuse bands, centred at ~0·034 and 0·21 Å^{-1} (Fig. 3, curve B); in other words, the lamellar structure "melts". Besides, recent e.s.r. experiments (Bruno, Cannistrano, Gliozzi, De Rosa & Gambacorta, unpublished results) suggest the presence of clusters of glycerol headgroups immediately above the melting point: these clusters disappear around 60 to 70°C.

In the presence of excess water, a similar lamellar phase is observed at low temperature; this phase also melts, although at higher temperature (~30°C). The small swelling ($a = 39{\cdot}4$ Å at 0°C) and the fact that the intensity of the lamellar reflections is almost independent of hydration indicate that the amount of water taken up by the lamellar phase is small; however, the degree of hydration cannot be determined in the absence of a more systematic study as a function of the water content. Gliozzi, Paoli, Pisani, Gliozzi, De Rosa & Gambacorta (unpublished results) have estimated the maximal hydration to be 2·8% by gravimetric experiments.

Table 1

Number of electrons and volumes

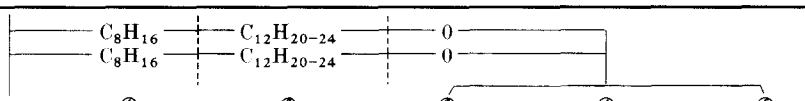

	①	②	③	④	⑤
n(e)	128·0	187·5	48·0	146·0	175·4
v(Å^3)	430·0	578·8	89·0	290·0	333·4

The lipid molecule is divided into 3 parts. ① The non-cyclic core; ②, the cyclopentane-containing end of the hydrocarbon chains (see Fig. 2); ③ the glycerol; and ④ the nonitol head of GDGT and GDNT; ⑤ is half the average polar group of the polar lipid extract (see the text). Volumes and number of electrons correspond to the average chemical composition. The volumes are estimated at 20°C by reference to a variety of chemical compounds. The temperature correction is assumed to take the form: $v_t = v_{20}[1 + (t-20)7{\cdot}48 \times 10^{-4}]$ (Tardieu *et al.*, 1973).

In the absence of water (the chemical composition is known in this case), the partial thickness d_{par} of the hydrocarbon layer can be determined, as well as the area per chain S_{ch} in the plane of the lamellae, using the formulae (see Table 1):

$$d_{par} = a v_{par}/v_{lip} = a(v_① + v_②)/(v_① + v_② + v_③) \quad (3)$$

$$S_{ch} = v_{lip}/(2a) = (v_① + v_② + v_③)/a. \quad (4)$$

At $t = -3$°C and with $a = 35{\cdot}9$ Å, the result is $d_{par} = 33{\cdot}0$ Å, $S_{ch} = 30{\cdot}1$ Å^2.

The relative intensity of the lamellar reflections, odd orders barely decreasing with increasing s, even orders weak or absent (see Fig. 4 legend), indicates that the electron density profile consists of two narrow peaks with similar content, one at $x = 0$ and one of opposite sign at $x = a/2$. In this case, the choice of the signs of the reflections is obvious. The Fourier transform is plotted in Figure 4. The positive and the negative peaks correspond to the parts ③ and ① of the molecule (see Table 1); their size and shape are consistent with the estimates of volumes and electron densities.

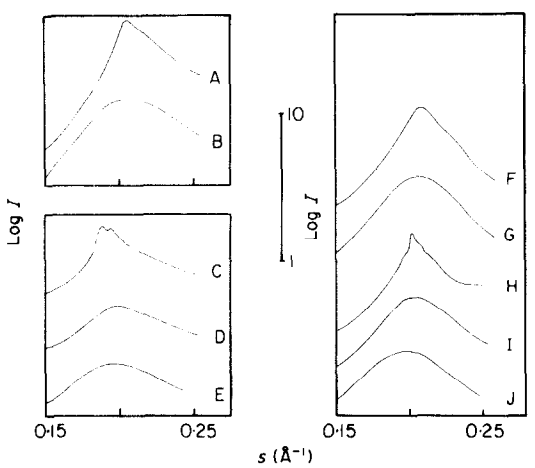

Figure 3. Intensity distribution in the high-angle region. The curves represent the logarithm of the microdensitometer tracings, the base-line being taken at an unexposed portion of the film. The vertical bar corresponds to a 10-fold intensity ratio.

Curve	Lipid	c	t (°C)	Phase
A	GDGT	1·0	−3	Lβ'
B	GDGT	1·0	20	Melt
C	TLE	0·65	20	Lβ'
D	TLE	0·65	72	Lα
E	TLE	0·70	96	Q^{230}
F	GDNT	1·0	0	P
G	GDNT	1·0	20	P
H	GDNT	<0·5	20	?
I	GDNT	0·90	20	Q^{230}
J	GDNT	0·90	79	H

The intensity distribution in the high-angle region suggests that the chains are stiff and probably tilted with respect to the normal to the plane of the lamellae (Tardieu *et al.*, 1973); in other words, the structure appears to be of type Lβ'. A more detailed analysis of the organization of the chains hinges upon a variety of factors (possible segregation of chemically different molecules in structurally different domains, symmetry and dimensions of the lattices, angle of tilt, electron density distribution along the chains; Tardieu *et al.*, 1973), whose effects are difficult to assess in the absence of additional information.

The angle of tilt γ and the cross-sectional area per chain Σ_{ch} can be expressed in terms of the partial thickness of the hydrocarbon layer d_{par} and of the fully extended length of the hydrocarbon chain D:

$$\cos\gamma = d_{par}/D \quad (5)$$

$$\Sigma_{ch} = S_{ch}\cos\gamma. \quad (6)$$

The fully extended length of an isoprenoid chain 32 carbon atoms long can be estimated to be 40 Å, by analogy with polyethylene (1·25 Å per —CH_2—); for an isoprenoid chain with an average of 2·3 cyclopentane groups, D can be assessed to be approximately 37 Å (see Fig. 2). Introducing this value and d_{par} (eqn (3)) in equation (5), we obtain $\gamma \approx 27°$ and $\Sigma_{ch} \approx 27$ Å^2. Note that, as expected, the cross-sectional area is larger for isoprenoid than for polyethylene chains (≈ 20 Å^2).

The fact is noteworthy that in GDGT (and not in the other lipids studied in this work) the long-range periodic order collapses as the short-range conformation of the chains becomes disordered. The absence of liquid-crystalline phases, and also the very small degree of hydration (these are direct consequences of the sharp segregation of the polar

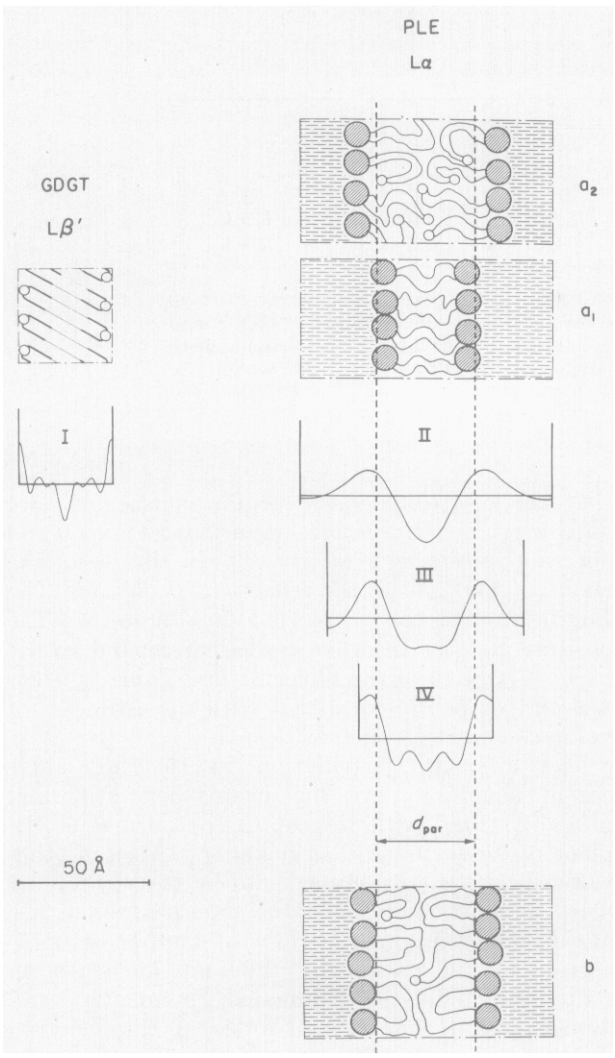

Figure 4. The structure of the lamellar phases. The small circles and the large hatched circles represent the unsubstituted glycerol and the substituted nonitol headgroups, respectively. The wriggles represent the chains in the α conformation, the straight segments represent the stiff chains in the β′ conformation. The water regions are lightly hatched. The electron density profiles correspond to the following experiments, structure factors and signs (see the text and Fig. 9):

	Lipid	Phase	c	t (°C)	a (Å)
I	GDGT	Lβ′	1·0	−3	35·9
II	PLE	Lα	0·52	70	97·7
III	PLE	Lα	0·67	70	76·1
IV	PLE	Lα	1·00	70	51·6
	$F(1)$	$F(2)$	$F(3)$	$F(4)$	$F(5)$
I	+2·89	0	+2·40	+0·72	+1·81
II	−3·20	−5·87	−2·04	0	0
III	−3·39	−4·79	+1·56	+1·07	0
IV	−4·50	+1·79	0	−1·52	0

GDGT: The positive and the negative electron density peaks correspond to the glycerol headgroups and to the segments of the chains devoid of cyclopentane groups, which are represented by a lighter line in the upper frame (see Fig. 2).

PLE: As discussed in Results, section (d) (i), 2 alternative structures can be proposed. One (upper frames) consists of 2 types of lamellar domains: a_1 is thinner than average and contains all the lipid molecules with substituted glycerol and nonitol headgroups; a_2 is thicker than average and contains the other lipid molecules, whose unsubstituted glycerol headgroups are embedded in the hydrocarbon matrix. The other structure, b (lower frame), consists of uniform and smooth lamellae, in which all the bipolar lipid molecules are U-shaped with the 2 headgroups anchored on the same side of the lamella. See Results, section (d) (i) for a discussion of the 2 structures.

headgroups away from the hydrocarbon medium) indicate that the glycerol headgroups of GDGT do not share the polar nature of the headgroups of amphiphilic lipids, and are more soluble in the hydrocarbon matrix than in the polar hydrated medium.

(c) *Glycerol dialkyl nonitol tetraether*

The portion of the phase diagram explored in this work is represented in Figure 5. Three phases, labelled P, Q^{230} and H, were identified; each phase was observed pure over the regions delimited in Figure 5. The intermediate regions containing two or more phases were not explored as carefully, with the exception of the high temperature–low concentration end containing the phase H and presumably water (small amounts of water are not detected by our experiments; see Materials and Methods).

Two intermediate regions cross-hatched in Figure 5 deserve a few comments. One, at the transition between P and H, will be discussed below. The other, at low temperature and high water content ($c < 0{\cdot}88$, $t < 30$°C) is characterized by fairly sharp high-angle reflections (see Fig. 3, curve H) and several not quite sharp small-angle reflections, sometimes resolved into a muddle of sharp lines; in addition, equilibrium is not easily attained in this region. In the absence of additional information, provided for example by chemically pure compounds, it is difficult to identify the phases involved and to determine their structure.

With the exception of the region discussed above, the hydrocarbon chains always take up a disordered conformation (type α), as shown by the presence of a diffuse band centred at $s \approx 0{\cdot}20$ Å^{-1} (Fig. 3).

(i) *Rectangular phase P*

This phase is characterized by six sharp small-angle reflections, which can all be indexed according to a two-dimensional centred rectangular lattice. The cell dimensions are reported in Figures 5 and 6 as a function of water content and temperature.

The structure of this phase (see Fig. 7) consists of lipid molecules oriented in the x direction, with the nonitrol headgroups located in flat ribbons parallel to $0y$ and of width $b/2$. The hydrocarbon chains take up a somewhat disordered conformation, and

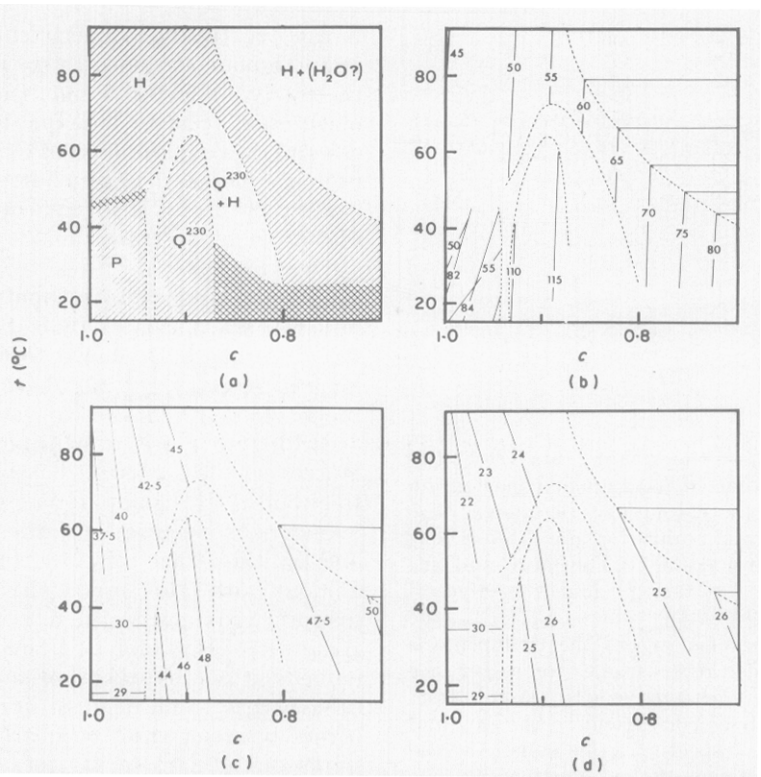

Figure 5. (a) Phase diagram of the system GDNT–water. The 1-phase regions are hatched: the cross-hatched regions are discussed in the text. The positions of the phase boundaries (dotted lines) are not known with great accuracy. The conformation of the chains is disordered in all the phases, with the exception of the cross-hatched region. (b) Lattice dimensions (in Å): parameter a for the phases H and Q, parameters a and b for the phase P. (c) Area per chain at the polar/apolar interface (S_{ch}, in Å^2), assuming (case A) that only the nonitol groups belong to the polar moiety. (d) as (c), assuming that both the nonitol and the glycerol groups are polar (case B).

the glycerol groups are less precisely localized than the nonitol groups: the disorder, both in the hydrocarbon chains and in the glycerol groups, increases as the temperature is raised. This structure is supported by the following arguments:

(1) The lattice parameter a is almost independent of temperature and its value is close to twice the extended length of the lipid molecule; b is much shorter and more variable.

(2) The presence of flat ribbons of width $b/2$ is based upon crystallographic arguments developed in Appendix 1.

(3) The section $\rho(x, 0)$ of the electron density distribution (see Fig. 7 and Appendix 1) displays positive and negative peaks corresponding to the nonitol and the glycerol headgroups, and to the segment of the hydrocarbon chains devoid of cycles, respectively (see Fig. 4 and Table 1).

(4) As the temperature rises, the high-angle band broadens (see Fig. 3, curves F and G), as well as the peak of the electron density profile corresponding to the glycerol groups (see Fig. 7).

The partial thickness of the ideal hydrocarbon ribbon parallel to the polar ribbon is:

$$d_{par} = (a/2)c_{v,par}. \qquad (7)$$

The area per chain at the surface of the ribbons can be determined, assuming that all the hydrocarbon chains, even those near the edge of the ribbons, are oriented almost parallel to $0x$:

$$S_{ch} = c_{par}/(2d_{par}). \qquad (8)$$

$c_{v,par}$ refers to the hydrocarbon moiety (① + ② in Table 1). Note (Fig. 6) that d_{par} is barely shorter than the fully extended length D, and that S_{ch} is

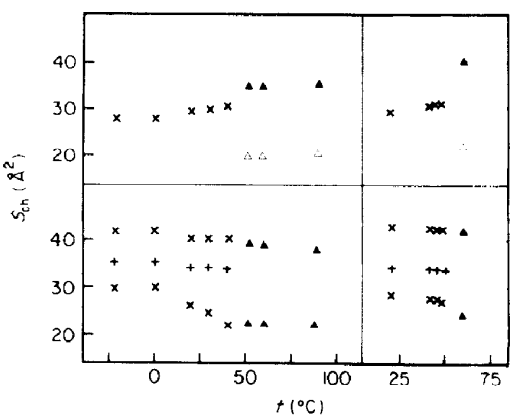

Figure 6. P/H phase transition in GDNT. The 2 experiments correspond to $c = 1$ (left) and $c = 0{\cdot}95$ (right). Lower frame: × represents half the lattice parameters of P, + represents the partial thickness of the hydrocarbon layer (eqn (7)); ▲ represents the spacings of the first 2 reflections of H ($\sqrt{3}\,a/2$, $a/2$). Upper frame: ×, area per chain in P (eqn. (8)); ▲ and △ are the area per chain in H for case A and B, respectively (see the text and eqns (11) and (12)). Note that the parameters of P appear to merge continuously into those of H as the temperature is raised.

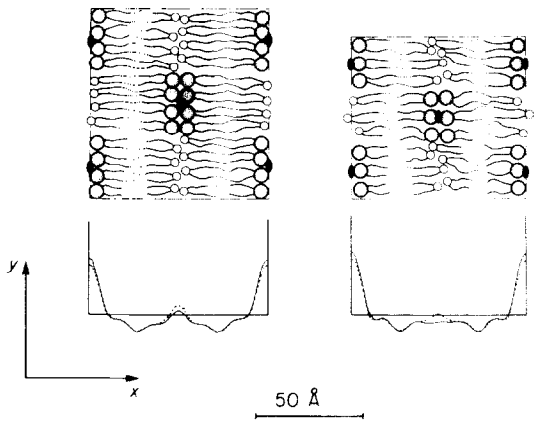

Figure 7. The structure of the phase P of GDNT. The 2-dimensional lattice is centred rectangular (space group cmm); the position of the 2-fold axes is shown. The experimental conditions and parameters are given below; left frames 0°C, right frames 30°C. The large and the small circles represent the nonitol and the glycerol groups, respectively; the wavy lines represent the hydrocarbon chains, thickened where the cyclopentane groups are present. The lower frames represent the section $\rho(x, 0)$ of the electron density distribution: continuous and broken lines correspond to the raw and the y-sharpened profiles, respectively (see eqns (A5) and (A6)). The amplitude and sign of the reflections are (see Appendix 1):

t (°C)	a (Å)	b (Å)	$F(2, 0)$	$F(4, 0)$
0	84·6	59·2	+39·4	+13·4
30	81·3	51·1	+32·2	+11·5

$F(6, 0)$	$F(1, 1)$	$F(3, 1)$	$F(5, 1)$
+8·9	+15·2	+6·1	+4·5
+7·7	+17·3	+8·9	+6·7

barely larger than the cross-section Σ_{ch} of the hydrocarbon chains ($D \sim 37$ Å, $\Sigma_{ch} \sim 27$ Å^2, see section (b), above).

We can thus conclude that in phase P the nonitol headgroups segregate away from the glycerols and from the hydrocarbon chains. Moreover, it appears that the disorder of the chains increases with rising temperature.

It may be noted that phases with a similar ribbon-like structure have been observed often in lipid–water systems (Luzzati, 1968; Tardieu *et al.*, 1973).

(ii) *Hexagonal phase H*

This phase is observed over an extended region of the phase diagram (see Fig. 5). Its X-ray scattering spectra contain several sharp small-angle reflections, whose reciprocal spacings ratios are $1 : \sqrt{3} : \sqrt{4} : \sqrt{7} : \sqrt{9} : \sqrt{12} : \sqrt{13}$. This sequence is consistent with a two-dimensional hexagonal lattice.

In fact, the two lattices H and P are never observed simultaneously, and the lattice dimensions seem to merge continuously into one another with varying temperature (see Fig. 6); therefore, the X-ray scattering experiments fail to provide unambiguous evidence as to whether P and H are thermodynamically distinct phases or two variants of the same phase. This question is settled by the calorimetric experiments of Gliozzi *et al.* (1983); the presence of a heat absorption peak near 38°C in the heating scan of GDNT indicates the existence of a first-order phase transition.

Two-dimensional hexagonal phases are commonly observed in lipid–water systems (for reviews, see Luzzati, 1968; Shipley, 1973). Their structure has been shown to consist of indefinitely long straight cylinders, whose section is presumed to be circular, parallel to each other and packed according to a two-dimensional hexagonal lattice. Moreover, the structure has been shown to belong to either of two types: in one, H_I, the interior of the cylinders is occupied by the hydrocarbon chains and in the other, H_{II}, by the polar moiety. By analogy with other lipids, the position in the phase diagram proximal to the dry end indicates that the structure of H is of type II; namely, polar cylinders embedded in a hydrocarbon matrix. The other type of structure would lead to unreasonably thin polar layers between the hydrocarbon cylinders and to unreasonably large areas per chain (see below).

In order to determine the dimensions of the structure elements we assume, as usual, that water and hydrocarbons do not mix and that the polar/apolar interface is covered by the polar groups of the lipid molecules. With regard to the partition of the glycerol and the nonitol groups between the polar and the apolar regions, we envisage two extreme situations.

Case A: *only the nonitol headgroups belong to the polar moiety; the glycerol headgroups do not mix with the nonitrol groups and are dispersed in the hydrocarbon matrix.*

Case B: *both the nonitol and the glycerol headgroups belong to the polar moiety.*

A variety of arguments show that alternative A is far more satisfactory than B.

(1) The observation that the lattice parameters of the phases P and H merge continuously into one another (Fig. 6) suggests that the cylinders of H originate from the ribbons of P, which in turn contain only the nonitol headgroups (Fig. 8).

(2) In GDGT, the glycerol headgroups appear to mix with the hydrocarbon chains when these take up a disordered conformation (see section (b), above; note that the melting temperature of GDGT is not far from the temperature of the P/H transition of GDNT; namely, 30°C and 45°C in the presence of 5% water).

(3) The third argument hinges upon the well-known rule that within and throughout any lipid–water system, and across all phase boundaries, the area per chain at the polar/apolar interface always increases, or at least never decreases, with increasing water content and/or increasing temperature. This rule is fulfilled in all the lipids studied so far, provided the separation of the lipid molecules into polar and apolar regions follows the convention

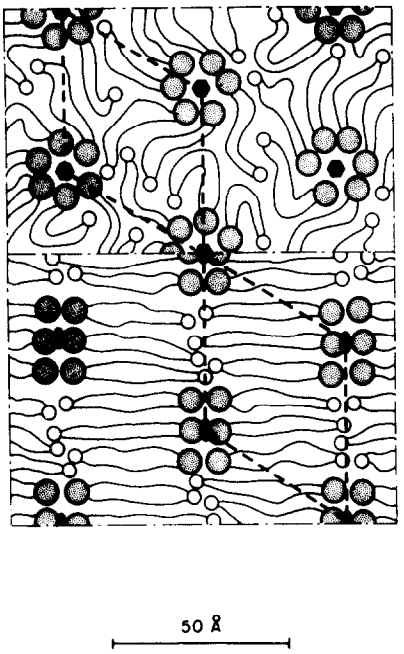

Figure 8. P/H phase transformation in GDNT. The lattices of the phases P and H ($c = 1$, $t = 14°C$ and $c = 1$, $t = 52°C$, respectively, see Fig. 5) are juxtaposed, with a schematic representation of the structures (see Figs 7 and 10). Apparently, the cylinders of H derive from the ribbons of P and thus contain only the nonitol groups, the glycerol groups being dispersed in the hydrocarbon matrix.

adopted in section (a), above (see Luzzati, 1968; Luzzati *et al.*, 1968*c*; Seddon *et al.*, 1984). The area per molecule, S_{mol}, at the surface of the rods can be determined as follows:

$$R = (3^{1/2}c_{v,pol}/2\pi)^{1/2}a \quad (9)$$

$$S_{mol} = 4\pi v_{par}R/[3^{1/2}c_{v,par}a^2], \quad (10)$$

where a is the parameter of the hexagonal cell, R is the radius of the polar rods. In case A, the subscripts pol and par refer, respectively, to water + nonitol and to hydrocarbon + glycerol, in case B to water + nonitol + glycerol and to hydrocarbon. The area per chain at the surface of the rod is:

$$S_{ch} = S_{mol}/2 \quad \text{in case A.} \quad (11)$$

$$S_{ch} = S_{mol}/4 \quad \text{in case B.} \quad (12)$$

The two values of S_{ch} are plotted in Figure 5 and reported in Table 2. Clearly, only in case A is the rule fulfilled; in case B, S_{ch} would become even smaller than the cross-section ($\Sigma_{ch} \sim 27$ Å^2).

We thus conclude that the polar cylinders contain only (or mainly) the nonitol groups and water, and that all (or most) of the glycerol groups are embedded in the hydrocarbon matrix.

This structure lends itself to an additional verification. Let us assume (at least to a first approximation) that at all water contents, the electron density distribution inside the polar cylinders is a radial function of the ratio r/R, and

Table 2

Some dimensions relevant to the hexagonal and to the cubic phases

Lipid phase	GDNT H		GDNT H		GDNT H	
t (°C)	90		70		41	
c	1·0		0·82		0·69	
a (Å)	44·9		64·6		83·6	
	A	B	A	B	A	B
$c_{v,pol}$	0·121	0·158	0·238	0·313	0·399	0·424
R (Å)	8·2	9·4	18·0	19·0	27·7	28·6
S_{ch} (Å^2)	37·2	21·3	47·8	25·1	51·2	26·4
L_{max} (Å)	17·7	16·5	19·2	18·3	20·5	19·7
L_{min} (Å)	14·2	13·1	14·3	13·3	14·1	13·2
Lipid Phase	GDNT Q^{230}		PLE Q^{230}		PLE Q^{224}	
t (°C)	50		95		95	
c	0·91		0·74†		0·58	
a (Å)	112		191		157	
	A	B	A	B	A	B
$c_{v,pol}$	0·203	0·236	0·446	0·457	0·572	0·581
R (Å)	10·5	11·4	27·7	28·0	41·5	42·3
S_{ch} (Å^2)	48·5	25·7	34·9	27·9	39·5	31·7
L_{max} (Å)	20·8	19·9	25·7	25·4	22·6	21·8
L_{min} (Å)	13·8	12·9	13·7	13·3	14·0	13·2

The nature of the lipid and the structure of the phase are specified in each case. c is the concentration, t the temperature, a the cell parameter, $c_{v,pol}$ the volume concentration of the polar moiety (eqn (1)), R the radius of the polar rods, S_{ch} the area per chain at the interface (eqns (11), (12), (16)), L_{max} the longest distance from any point in the hydrocarbon matrix to the surface of the rods and L_{min} half the minimum distance between 2 unconnected rods. For the hexagonal phase, $L_{max} = a/(2\cos 30°) - R$, $L_{min} = a/2 - R$; for the cubic phases, see Appendix 2. Cases A and B are discussed in Results, section (c) (ii). The 3 examples of hexagonal phases are those of Fig. 10.

† Although in this experiment the phase Q^{230} is not pure (see Fig. 11), we assume that its concentration coincides with the nominal concentration, on the grounds that the other phase (Lα) is present in trace amounts.

that the electron density is fairly uniform outside the cylinders. In this case, we expect that at all concentrations the structure factors will sample a continuous function of the product sR. Figure 9 shows that the data fulfil this expectation and specifies the sign of the structure factors. Three examples of electron density distributions corresponding to different degrees of hydration are plotted in Figure 10, along with a schematic representation of the structure. The agreement is excellent.

It must be noted that the electron density contrast associated with the glycerol headgroups is so weak (see Table 1) that in the presence of the much denser nonitol groups the intensity of the reflections is not sensitive to the location of the glycerols. This unfortunate circumstance precludes any direct crystallographic determination of the position of the glycerol headgroups.

(iii) *Cubic phase* Q^{230}

The identification of this phase and its structure is discussed in Appendix 2.

Arguments analogous to those invoked in the discussion of phase H show that the structure is most likely of type II. The question of the partition of the glycerol and the nonitol groups between the polar and the apolar regions also can be discussed along similar lines. The structure consists of 24 identical rods of length l and of radius R, bevel-shaped at each end. The expressions of the volume ϕ and of the area σ of one rod are given in Appendix 2 (eqns (A7) and (A8)). When $c_{v,pol}$ and a are known, one can solve the equation:

$$c_{v,pol} = 24\phi/a^3, \tag{13}$$

into R (see eqn (A7)), determine the area per molecule at the polar/apolar interface (see eqn (A8)):

$$S_{mol} = \sigma r_{pol}/\phi, \tag{14}$$

and, finally, the area per chain using equation (11) in case A and equation (12) in case B.

The results are shown in Figure 5 and in Table 2. Clearly, case B is utterly at variance with the rule that S_{ch} must not increase as c increases. Case A is in better agreement with that rule, although the largest values for Q^{230} slightly exceed the smallest values for H. One possible explanation of this anomaly is that, in reality, the junction of the three rods is smoother, and consequently the area smaller, than in the simplified model used for the calculation of S_{ch}. However, the possibility cannot be ruled out that the partition of the glycerol groups between the polar and the apolar regions is not as extreme as in the cases A and B considered above. The conclusion is clear, though, that in both H and Q^{230} most, if not all, of the glycerol groups are embedded in the hydrocarbon matrix.

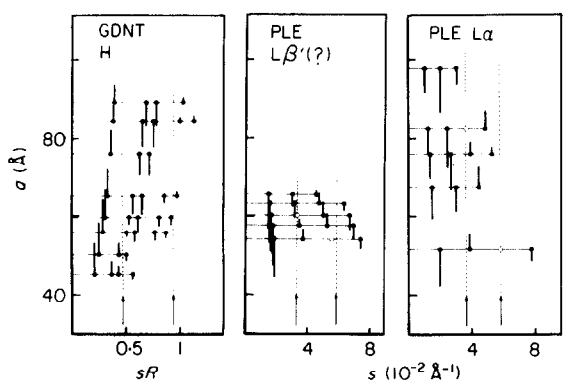

Figure 9. Analysis of the amplitude of the reflections. Each experiment is identified by a horizontal line whose ordinate is the lattice parameter a. The vertical bars are proportional to the observed amplitudes of the reflections: the open circles represent reflections whose intensity is too weak to be observed. Phase H of GDNT: the abscissae are the product of the s value of the reflection and of the radius R of the polar cylinders (see Results, section (c) (ii)). Lamellar phases of PLE: the abscissae are the s values of the reflections (note that, for the same repeat distance a, the amplitudes of the reflections of TLE are indistinguishable from those of PLE; note also that the phase Lα with $a = 51{\cdot}6$ Å is not observed pure). The general trend of the 3 phases is consistent with the notion that in each case the structure factors sample a unique continuous curve, whose zeros are shown by the vertical arrows. Note also that the lattice disorder increases with increasing water concentration (namely, the intensity cut-off shifts to small s values as a increases).

(d) *Total and polar lipid extracts*

The regions of the phase diagrams explored in this work and the position of the different phases are presented in Figure 11. Thermodynamic equilibrium is unusually difficult to attain in the transitions involving the cubic phases. This problem (which we discuss below), along with the scarcity of lipids available, made the exploration of these phase diagrams quite tricky and prevented a satisfactory delimitation of the domains of the cubic phases. Moreover, complex phenomena were observed at low temperature and high water content (see below).

The two phase diagrams are similar: the same phases are present, in the same relative position. The overall low temperature shift of the phase diagram of TLE with respect to that of PLE shows that the chemical composition of the phases is not quite the same in the two lipids and thus that at least a fraction of the non-polar lipids is incorporated in the ordered phases of TLE. Also, arguments discussed below suggest that additional, and poorly ordered phase(s) are present in the TLE–water system (? in Fig. 11).

(i) *Lamellar phase Lα*

This phase displays the diffuse high-angle band characteristic of hydrocarbon chains in the α conformation (Fig. 3, curve D) and a few small-angle reflections, not quite as sharp as those of other phases, whose spacing ratios are those of

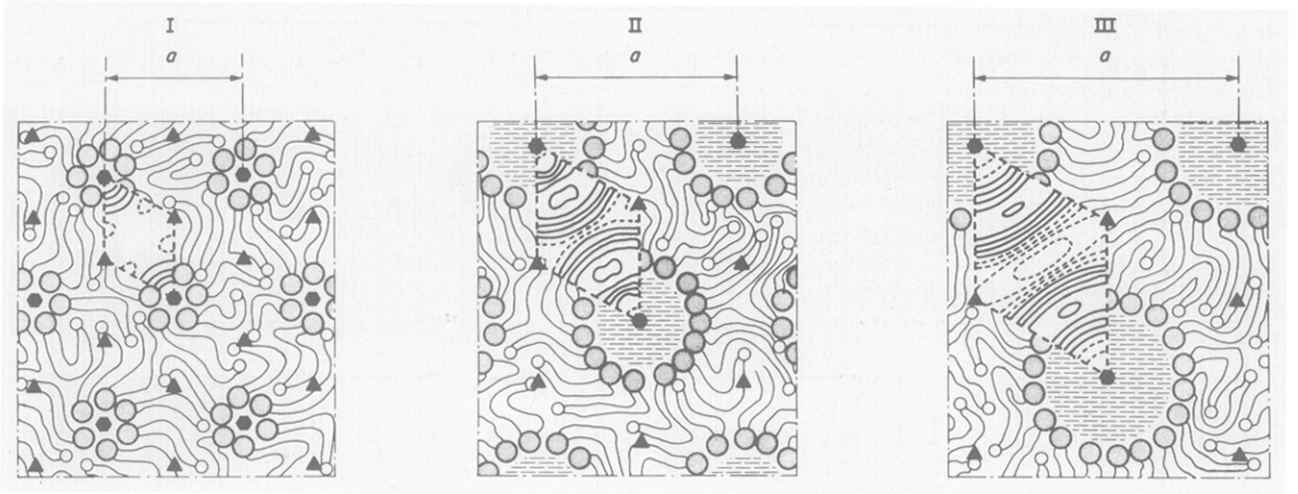

Figure 10. Structure of the phase H of GDNT. Symbols as in Figs 4 and 6, and positions of the 6- and the 3-fold axes. The structure is supposed to consist of circular cylinders containing the polar moiety (water and nonitol groups); the glycerol groups are dispersed in the hydrocarbon regions. The electron density distribution is represented in the insets: the scale is arbitrary, the density lines are equally spaced, the negative values are dotted. The amplitudes and the signs (see Fig. 9) of the reflections are:

	c	t (°C)	a (Å)	$F(1,0)$	$F(2,1)$	$F(2,0)$	$F(3,1)$	$F(3,0)$
I	1·00	90	44·9	+87·3	+38·2	+24·9	−10·2	0
II	0·82	70	64·6	+72·1	−41·9	−50·2	−16·7	+15·5
III	0·69	41	83·6	+42·0	−62·1	−60·8	+12·8	+18·7

lamellar structures. Some diffuse scattering is present also in the small-angle region.

In PLE, the partial thickness of the lipid layer (proportional to d_{par}, see Fig. 12) is independent of c and the intensities of the reflections seem, at all values of the repeat distance, to sample a unique function of s (Fig. 9). These observations suggest that the structure of the lipid lamellae is independent of c. The plot in Figure 9 can be used also to ascribe signs to the reflections and thus to calculate the electron density profiles (Fig. 4).

With regard to TLE, the relative intensity of the reflections is the same as in PLE for the same repeat distance, in keeping with the notion that the structure of the lamellae is the same in the two systems. However, the concentration dependence of the repeat distance of TLE is at variance with that of PLE (Fig. 12). The most likely explanation of this anomaly is the presence in the TLE–water system of at least one additional disordered phase (which escapes detection).

A substantial fraction (41%, see section (a), above) of the lipid molecules contains one unsubstituted glycerol head. Therefore (see section (c), above) we must consider the two alternatives of the glycerol groups being either dispersed in the hydrocarbon matrix (case A) or located in the polar regions (case B). For the two alternatives, we calculate d_{par} and S_{ch} using the expressions:

$$d_{par} = ac_{v,\,par} \tag{15}$$

$$S_{ch} = 2v_{par}/(\chi d_{par}), \tag{16}$$

where a is the repeat distance, $c_{v,\,par}$ is the volume concentration defined in equations (1) and (2), and χ is the average number (per lipid molecule) of chain ends at the polar/apolar interface. According to the chemical composition (see section (a) and Table 1), the parameters involved in equations (1), (15) and (16) take the values: $v_{par} = 2054{\cdot}0$, $v_{pol} = 630{\cdot}3$, $\chi = 3{\cdot}18$ in case A; $v_{par} = 2017{\cdot}6$, $v_{pol} = 666{\cdot}7$, $\chi = 4$ in case B. The values of a, d_{par} and S_{ch} are plotted in Figure 12 as a function of c (with regard to d_{par}, the differences between cases A and B are negligible).

In case B, the value of S_{ch} is so small that it is not compatible with lipid lamellae containing disordered chains ($S_{ch} = 27$ Å^2, equal to the cross-sectional area of one chain). In case A, on the contrary, the value of S_{ch} is consistent with chains in the α conformation (compare with GDNT, Fig. 5). We thus conclude that in the phase Lα of PLE (and of TLE), as in the phases H and Q^{230} of GDNT, the unsubstituted glycerol headgroups are embedded in the hydrocarbon matrix.

A most surprising feature of this phase is the partial thickness of the hydrocarbon layer (39 Å, see Fig. 12) being somewhat larger than the fully extended length of the hydrocarbon chains (37 Å, see section (b), above), rather than substantially smaller, as in the Lα phase of all the lipids studied so far (see also the low temperature phase below).

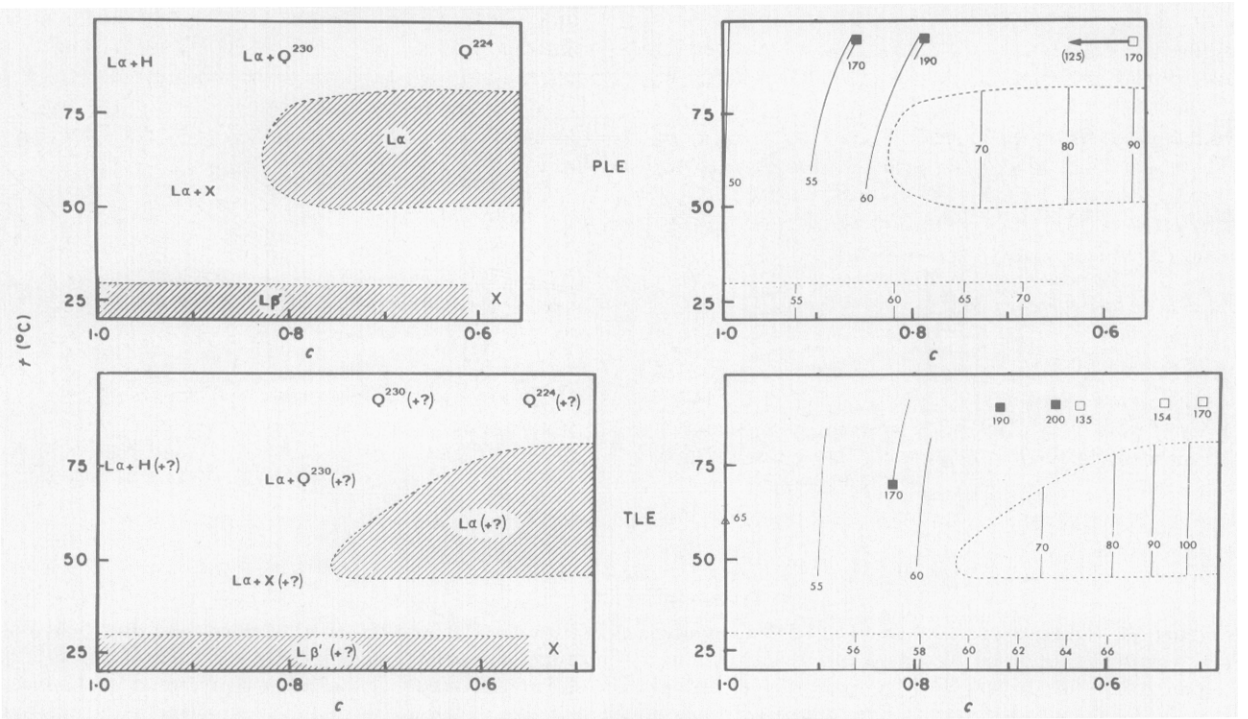

Figure 11. Left frames. Phase diagrams of the systems PLE–water and TLE–water. The 1-phase regions are hatched. the position of the phase boundaries was not determined with great accuracy. In addition, the pronounced metastability of the cubic phases (see the text) prevented a proper location of the phase boundaries. In the case of TLE, arguments discussed in the text suggest the presence of some additional disordered phase, identified by a question mark. X shows the presence of unidentified sharp reflections. Right frames. Lattice dimensions (in Å) of the lamellar, hexagonal (△), cubic Q^{230} (■) and cubic Q^{224} (□) phases. Only one example of the phase Q^{224} of PLE is reported. The lipid–water sample, initially at $c = 0{\cdot}58$, was dried progressively; X-ray scattering experiments performed at various stages of the drying process (and without a control of concentration) showed that the structure was of type Q^{224} and that the lattice parameter had shrunk progressively from 170 to 125 Å (see the arrow in the top-right frame).

As a consequence, wherever a molecule spans the lipid membrane, the local thickness is smaller than average; some thickening elsewhere must compensate for that thinning. We can propose two types of structures consistent with this observation.

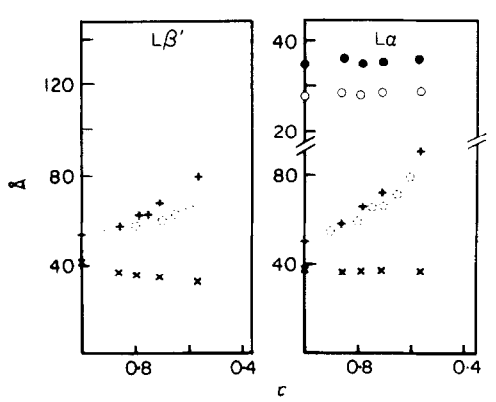

Figure 12. Some dimensions of the lamellar phases of PLE. The data refer to experiments performed at 20°C (Lβ') and 70°C (Lα). +, Repeat distance; ×, partial thickness of the hydrocarbon layer (eqn (15)); ●, area per chain in case A; ○, in case B (eqn (16)). The broken circles plot the repeat distance of TLE *versus* the nominal concentration, which may differ in this case from the concentration of the lamellar phase (see the text).

(1) The phase contains a heterogeneous mixture of the two types of lamellar domains: one domain (a_1 in Fig. 4) consists of a monolayer of bipolar molecules (those whose two headgroups are substituted glycerol and nonitol) spanning the lipid layer; the other domain (a_2 in Fig. 4) is a bilayer of the other class of molecules, with the unsubstituted glycerol headgroups embedded in the hydrocarbon matrix. The lamellar structure could be a statistical alternation of two kinds of uniform lamellae (one entirely of type a_1, the other of type a_2), or else be an ordered stacking of heterogeneous lamellae, each being a patchwork of the two types of domains. Note that these structures require that the unsubstituted glycerol headgroups be immiscible with the polar medium (case A, above).

(2) All the lamellae are smooth and homogeneous. The only way to avoid thickness fluctuations is to assume that all the bipolar lipid molecules are U-shaped, with the two headgroups located on the same side of the lamella (b in Fig. 4). Note that this type of structure can, in principle, accommodate any distribution of the unsubstituted glycerol headgroups (although the arguments discussed above point in favour of case A).

The structure of type a, with possibly a fraction of U-shaped lipid molecules, is consistent with the lack of sharpness of the lamellar reflections and

with the presence of diffuse scattering at small angles. The structure of type b would entail the presence of an electron density trough in the middle of the hydrocarbon layer, which is totally absent from the profiles in Figure 4 (especially in profile IV, whose resolution is highest). Further experiments are needed to settle this issue and to determine the relative distribution of the two types of domains (see also subsection (ii), below).

(ii) *Low temperature phase*

This phase displays fairly sharp high-angle reflections (Fig. 3, curve C), whose shape and position are barely dependent on concentration, and a few not quite sharp small-angle reflections accompanied by some diffuse scattering. The values of a and d_{par} (eqn (15)) are plotted in Figure 12. The observation in PLE that d_{par} decreases slowly with increasing hydration and the presence of sharp high-angle reflections suggest that the phase is of type Lβ' and that the angle of tilt of the chains increases as c decreases (Tardieu *et al.*, 1973; Janiak *et al.*, 1976).

As in the phase Lα, the amplitude of the reflections plotted as a function of the repeat distance seems to sample a unique function of s, the same for PLE and TLE (Fig. 9). This observation suggests that the structure of the lamellae is almost independent of c (note that d_{par} barely varies over the observed range of c: Fig. 12) and that it is the same in the two systems. However, as for the phase Lα, the a *versus* c dependence of TLE is at variance with that of PLE, again suggesting the presence of an additional disordered phase in TLE. The electron density profiles (not shown) are very similar to those of the phase Lα.

Although the properties discussed so far are those of a lamellar phase, a few anomalies point to an organization more complex than a plain stacking of uniform lipid lamellae. One is the abnormal value of d_{par} at $c = 1$ (41 Å), too large to be compatible with a monolayer of lipid molecules ($d_{par} \leq 37$ Å in this case, see section (b), above). The other is the presence at high water content of unidentified families of sharp small-angle reflections incompatible with a lamellar phase. An explanation must probably be sought in modulations of the lamellar structure analogous to those commonly observed in lipids (phases Pβ', Lγ, Pγ, L$\alpha\beta$, Paβ; see Luzzati & Tardieu, 1974). There are too many parameters involved (partition of the unsubstituted glycerol groups, relative proportion of chains in the α and in the β conformations, corrugation of the stiff chains domains) and the data are too scanty to justify a more detailed analysis of this phenomenon.

(iii) *Hexagonal phase II*

In both TLE and PLE, a hexagonal phase is observed over a fairly narrow region of the phase diagram, near the high-temperature, low-water end. This phase is never found pure, although its relative amount increases with increasing temperature and with increasing lipid concentration, and thus neither its chemical composition nor the dimensions of its structure elements can be determined. By analogy with other lipids (Luzzati, 1968) the position of the phase H near the dry end of the phase diagram indicates that its structure is of type II.

(iv) *Cubic phases Q^{230} and Q^{224}*

The two lipid–water systems TLE and PLE display, at high temperature, the two cubic phases Q^{230} and Q^{224} (Fig. 11). The identification of these phases as well as their structure are described in Appendix 2.

The two structures consist of rods, and the two alternatives, hydrocarbons inside (type I) or outside (type II) the rods, are topologically distinct. A variety of arguments indicate that the structures are most likely of type II; namely, the analogy with GDNT (see section (c), (ii), above), the presence of the phase H_{II} on the dry side of the cubic phases, the fact that in other lipid–water systems the same cubic phases observed over a similar concentration range have been shown to be of type II (Longley & McIntosh, 1983; Larsson, 1983).

The question can also be asked whether the unsubstituted glycerol groups are located in the hydrocarbon (case A) or in the polar (case B) regions. The area per chain can be calculated in the two cases:

$$S_{ch} = S_{mol}/\chi. \qquad (17)$$

where S_{mol} is the area per molecule (see eqns (14) and (16)). The results, reported in Table 2, show that case A is in better agreement with the rule that S_{ch} increases as c decreases and/or t rises (see also Fig. 12). Moreover, the fact that L_{max} (Table 2) exceeds half the maximal length of the chains ($\sim$20 Å in the absence of cyclopentane groups, section (b), above) indicates that some of the lipid molecules must have at least one of their ends embedded in the hydrocarbon matrix if the space between the rods is to be filled efficiently.

The two cubic phases of TLE and PLE display a remarkable degree of metastability. Whenever a lipid–water sample adopts either cubic phase (for example in a heating scan), that structure sets in almost irreversibly; if the sample is subsequently brought back and kept at lower temperature, it may take weeks before the cubic phase gives way to the phase that was observed at that temperature in the initial heating scan. Eventually, though, the non-cubic phase is recovered and the thermal cycle can be scanned again: in other words, the phenomenon is not a consequence of a subtle irreversible degradation of the sample escaping chemical detection (see Materials and Methods). Such a degree of metastability is most unusual in lipid–water systems: all the examples of metastable structural transitions reported so far involve at least one phase with chains in an ordered conformation, whereas all the transitions between chains in the α conformation are fast. This phenomenon can be explained by the interplay of

the chemical structure of the lipid molecules and of the physical structure of the cubic phases. On the one hand, indeed, the polar groups are anchored on surfaces belonging to the two unconnected systems of rods; on the other hand, the two polar ends of most of the lipid molecules are attached each to one of the two networks. Under these conditions, the migration of the lipid molecules is limited by the diffusion of its two ends and by the entanglement of the chains: therefore, any phase transition involving long-range diffusion of lipid molecules is likely to be very slow. Obviously, this phenomenon does not concern lipid molecules with only one polar head.

4. Conclusions and Discussion

It is proper to stress the exploratory character of this work and to point out that the minute amounts of lipids available set severe experimental limitations. In spite of this shortcoming, all the facts reported are based upon repeated observations; we are not as sure, yet, not to have missed some phase, especially in the intermediate regions of the phase diagrams.

For the sake of clarity, we discuss separately the physico-chemical aspects of our work and its possible biological significance.

(a) *Physico-chemical aspects*

In the bipolar isopranyl lipids studied in this work, as in other lipids, the hydrocarbon chains are found to adopt two main types of short-range conformations. One (type α), predominant at high temperature, is highly disordered, more like in a liquid than in a solid (Luzzati, 1968). This conformation is characterized by a diffuse scattering band, similar in shape to that of fatty acid lipids but shifted to smaller angles, in keeping with the increased bulkiness of the chains (see Fig. 3). The other (type β'), predominant at low temperature, corresponds to stiff chains, parallel to each other and organized with rotational disorder according to a two-dimensional lattice. Apparently, the presence of side methyl groups and of isopentane cycles is compatible with this conformation, much like the presence of double bonds in fatty acid chains.

As usual in lipids, the phases with stiff chains consist of lamellae (we mention in Results, section (d) possible modulations of the lamellae). Melting the chains gives way to a variety of phases of widely different structures. This type of polymorphism is perhaps the most characteristic property of lipids, not shared by any other family of chemical compounds to nearly the same extent. One paradoxical feature of these structures is the ability to achieve a high degree of long-range order and yet to display an extremely disordered short-range conformation. It is worth pointing out, in this respect, that in physical systems, long-range order is usually the propagation of short-range order. From a heuristic viewpoint, the structure of this class of compounds should be visualized as a mutual organization of two unconnected continuums, one polar, one apolar, rather than described in terms of precise atomic positions (Luzzati & Tardieu, 1974).

Determining the structure of these phases is a game whose rules are worth discussing. As a consequence of the short-range disorder, the intensity of the reflections fades away rather sharply with increasing scattering angles, long before reaching atomic resolution. Under these conditions, the number of observed reflections is small, indexing is not a problem, and consequently attempts to improve the information by orientation and crystallization are fruitless. It is much more rewarding to alter the physical and the chemical parameters (in this work, temperature and water concentration) and to explore the phase diagrams carefully. The evolution of the structure parameters, the comparison with similar systems and the crystallographic analysis, all provide equally important arguments for the sake of proposing and testing structures. Although it would be next to impossible to prove that any structure is unique, it is rewarding to note that the structures put forward in the past, and thus the strength of the arguments, have withstood successfully the test of time.

All these comments have a general character; we may discuss now some specific aspects of bipolar isopranyl ether lipids. Four lipid preparations were studied in this work.

The symmetric hydrolytic fraction GDGT is virtually immiscible with water, and it displays only one lamellar phase with stiff chains. The fact is noteworthy that melting of the chains in this lipid is accompanied by the collapse of the periodic long-range organization, as if the glycerol headgroups then became miscible with the disordered hydrocarbons.

The asymmetric hydrolytic fraction GDNT is much more miscible with water. Apparently, the chains adopt an ordered conformation, even at low temperature, only when some water is present; the number and the structure of the phases with stiff chains was difficult to assess. There are three phases with disordered chains: H, Q^{230} and P. An interesting aspect of these phases (see below) is the partition of the glycerol headgroups.

The phase diagram of the polar lipid extract (PLE) is similar to that of other lipid extracts: one or more low temperature phases of type β with variable water content: hexagonal, cubic and lamellar phases at higher temperature, with chains in the α conformation. Two phenomena observed in this system are novelties in lipids: the metastability of the cubic phases and the partition of the unsubstituted glycerol headgroups. We discuss these phenomena more extensively below.

With regard to the total lipid extract (TLE), its phase diagram is similar to that of PLE. Yet, the difficulty of assessing the amount and the nature of the non-polar components present in each phase prevents the structure of the phases from being analysed properly.

The cubic phases deserve a few comments. As pointed out in Appendix 2, phases with this symmetry are commonly observed in lipid–water systems. The novelty of PLE and TLE is that the cubic phases are almost irreversible. As discussed in Results, section (d) (iii), the presence of this phenomenon in bipolar lipids, and its absence in other lipids, can be explained by the structure of the phases (the two consist of two three-dimensional networks of rods, intertwined and unconnected) and by the fact that the two polar heads of most bipolar lipid molecules are each anchored on one of the two different networks. An interesting question, related to the partition of the glycerol headgroups, is whether the cubic phase of GDNT is also metastable; the lack of a transition from the cubic to some other, lower temperature phase precludes any satisfactory answer (note that the temperature-induced $Q^{230} \rightleftharpoons H$ transitions are fast in both directions).

Another peculiar property of biradical lipids, not shared by other lipids, is the partition of some of the headgroups between the polar regions and the hydrocarbon matrix. A variety of arguments developed in Results, sections (c) and (d), lead us to conclude that in the GDNT and the PLE phases with disordered chains the unsubstituted glycerol headgroups are embedded in the hydrocarbon matrix rather than located in the polar regions along with the other headgroups. The observation that the area per chain, the most useful parameter in this type of analysis, appears to be larger in GDNT than in PLE (see Figs 5 and 12 and Table 2) might indicate that the partition is less completely in favour of the apolar regions in GDNT than in the model used to determine S_{ch} (note that the assumption that a small fraction of the glycerol headgroups is located in the polar regions suffices to remove the discrepancy). Yet, and by analogy with other lipids, S_{ch} may well vary with the nature of the polar groups.

(b) *Biological considerations*

Upon comparing the major molecular components of archaebacteria, prokaryotes and eukaryotes, one is struck by the extensive chemical differences observed in the lipids, especially by contrast with other components (nucleic acids, proteins, etc.) whose essential chemical features are preserved throughout all living organisms (Woese, 1981). The differences are in fact so large that one may wonder what bipolar isopranyl ether lipids have in common with monopolar fatty acid lipids (see Fig. 1). One element of the answer stems from this work: polymorphism. The similarity is indeed remarkable between the structural properties of the lipids extracted from *S. solfataricus* and those of the complex lipid extracts from other organisms: the hydrocarbon chains adopt similar conformations, and the same phases occupy the same relative positions in the phase diagrams (see bovine mitochondria, Gulik-Krzywicki *et al.*, 1967; human erythrocytes, Rand & Luzzati, 1968; chloroplasts, Rivas & Luzzati, 1969; bovine retinal rods, Huynh, 1973).

On the other hand, one difference is noteworthy. In the phase diagrams of lipid extracts from ordinary organisms (i.e. not archaebacteria), the lamellar phase Lα is predominant over the temperature–concentration range close to "physiological" conditions, whereas the other phases (H, Q, etc.) are encountered at higher temperature and at lower water content. This observation has often been invoked to dispose of the non-lamellar phases as mere crystallographic oddities having no biological relevance. By contrast, the phases of *S. solfataricus* lipids predominant under similarly "physiological" conditions (85°C in this case) are the rod-containing phases (H, Q^{230}, Q^{224}); even more extraordinary is the presence in these conditions of the two cubic phases, probably the most complex of all lipid organizations.

Thus, the properties of bipolar isopranyl lipids strengthen the long-standing suggestion that lipid polymorphism deserves biological consideration (see Introduction). The core of the argument is that the organization of the lipids in membranes is likely to undergo conspicuous fluctuations, rather than to be frozen in any particular structure, and that these structural fluctuations, localized in time and space and probably related to fluctuations in chemical composition, may well be involved in specific physiological events (see reviews by Luzzati, 1981; Rand, 1981; de Kruijff *et al.*, 1984). The observations reported here, besides emphasizing the ability of lipids to undergo polymorphic transitions also stress the remarkable variety of the structures built of rod-like elements: hexagonal organization of indefinitely long rods, two-dimensional networks with hexagonal or tetragonal symmetry (phases R and T. Luzzati *et al.*, 1968*a*), cubic organizations of three-dimensional networks (phases Q^{230} and Q^{224}). (We can also mention the phase Q^{223} reported by Tardieu & Luzzati (1970), some protein–lipid–water phases observed by Ericsson *et al.* (1983), and some unpublished observations by Gulik-Krzywicki.) One may thus wonder (see Luzzati *et al.*, 1968*b*) whether a flexible fabric of lipid threads with proteins inserted in the interstices would not provide a more realistic picture of membranes than an inert bilayer, especially with respect to the specialized regions that are involved in active physiological processes.

Too little is known about the architecture of *S. solfataricus* membranes to seek straightforward correlations with the structure of the lipid–water phases. Yet, two properties not shared with other lipids suggest a few comments.

The first is the presence in some lipid molecules of unsubstituted glycerol headgroups and the affinity of these groups for the hydrocarbon matrix. The precise distribution of these headgroups, especially with respect to the proteins, and the local thickening of the hydrocarbon layer due to their presence (note that these lipid molecules could span a hydrocarbon gap as wide as 75 Å) may well be

related to the growth conditions of thermoacidophilic archaebacteria. Besides, it is worth pointing out that, in agreement with the notion that the unsubstituted glycerol groups do not behave as polar headgroups, biphytanyl glycerol is not present (or at most in trace amounts) among the monopolar isopranyl lipids of other archaebacteria (Kates & Kushwaha, 1978; Kushwaha *et al.*, 1982).

The second property is the extraordinary metastability observed in the cubic phases. The possibility can be contemplated that the organization *in situ* of at least some of the lipids is analogous to that of the cubic phases; more precisely, that the two polar heads of one lipid molecule are anchored on two different surfaces, each belonging to one of two unconnected networks (in membranes, these networks may include proteins as well as lipids). Under these conditions, the migration of lipid molecules may be a very slow process, strongly limiting the rate of the high to low temperature structural transitions. This phenomenon could have the effect of preserving metastably the high-temperature structure of the membrane and thus of protecting the organism against extensive and durable temperature changes. Since the natural habitat of thermoacidophilic archaebacteria (see Fliermans & Brock, 1972; Brock, 1978; Langworthy, 1982) is likely to undergo frequent and extensive thermal fluctuations, bipolar lipids might well provide an evolutionary response to that challenge (note, in this respect, the remarkable correlation between the growth temperature of different archaebacteria and the concentration of bipolar lipids; Langworthy, 1982).

As a final comment, it is worth noting that in *S. solfataricus* lipids, as in lipid extracts from other organisms, the conformation of the hydrocarbon chains is predominantly disordered under physiological conditions.

Appendix 1

The Structure of the Phase P of Glycerol Dialkyl Nonitol Tetraether

It may be noted that all the observed reflections belong to two rows (h, 0 and h, 1, see the legend to Fig. 7). This particular intensity distribution suggests that the electron density fulfils, at least at low resolution, the following condition (besides those required by the space group):

$$\rho(x, y) = \rho_1(x)L(y) \tag{A1a}$$

$$L(y) = \begin{cases} 1 & -1/4 \le y \le 1/4 \\ 0 & \text{elsewhere} \end{cases}. \tag{A1b}$$

Indeed, in this case the expression of the structure factors takes the form:

$$F(h, k) = \int_0^{1/2}\int_0^{1/2} \rho(x, y) \cos 2\pi hx \cos 2\pi ky \, dx \, dy$$

$$= f(h)(\sin \pi k/2)/(2\pi k), \tag{A2a}$$

$$f(h) = \int_0^{1/2} \rho_1(x) \cos 2\pi hx \, dz, \tag{A2b}$$

$$F(h, 0) = f(h)/4, \tag{A2c}$$

$$F(h, k) = \begin{cases} 0 & \text{if } k \text{ even} \\ (-1)^{(k-1)/2} f(h)/(2\pi k) & \text{if } k \text{ odd.} \end{cases} \tag{A2d, A2e}$$

and the intensity of all the reflections with k even and $\neq 0$ is zero. Moreover, it can be verified that the intensity of all the reflections with k odd and >1 (see A2e):

$$I(h, k) = k^{-2} I(h, 1) \quad k \text{ odd}, \tag{A3}$$

turns out to be too small to be observed in our experiments.

With the moduli of the reflections and a chosen set of signs, one can calculate the two-dimensional electron density distributions $\rho(x, y)$. If, moreover, condition (A1) is fulfilled, then it is possible to determine the values of all the $F(h, k)$ terms for which $F(h, 1)$ is known (see (A2e)):

$$F(h, k) = k^{-1}(-1)^{(k-1)/2} F(h, 1) \tag{A4}$$

The sections $y = 0$ of the two types of electron density distributions are plotted in Figure 7. One corresponds to the raw data:

$$\rho(x, 0) = \sum_{h=1}^{6} \left[\sum_{k=-1}^{1} F(h, k) \right] \cos 2\pi hx, \tag{A5}$$

the other to the extrapolated values (see (A4)):

$$\rho_{y\text{-sharp}}(x, 0) =$$

$$\sum_{h=1}^{6} \{F(h, 0) + 2F(h, 1)[1 - 1/3 + 1/5 + \ldots]\}$$

$$\cos 2\pi hx =$$

$$\sum_{h=1}^{6} [F(h, 0) + \pi F(h, 1)/2] \cos 2\pi hx. \tag{A6}$$

The second profile may be called y-sharpened, as indeed the extrapolation in reciprocal space is equivalent to sharpening the electron density in the y direction. Naturally, the series termination effects in the x direction are present in the two profiles.

The signs are all chosen positive in keeping with the presence at the origin of the sharp peak associated with the nonitol groups. Other sign combinations were also tested: the results are far less satisfactory.

Appendix 2

The Structure of the Cubic Phases

Several phases have been observed in lipid–water systems whose long-range organization is highly ordered according to three-dimensional lattices, which belong to the cubic system. Tardieu (1972)

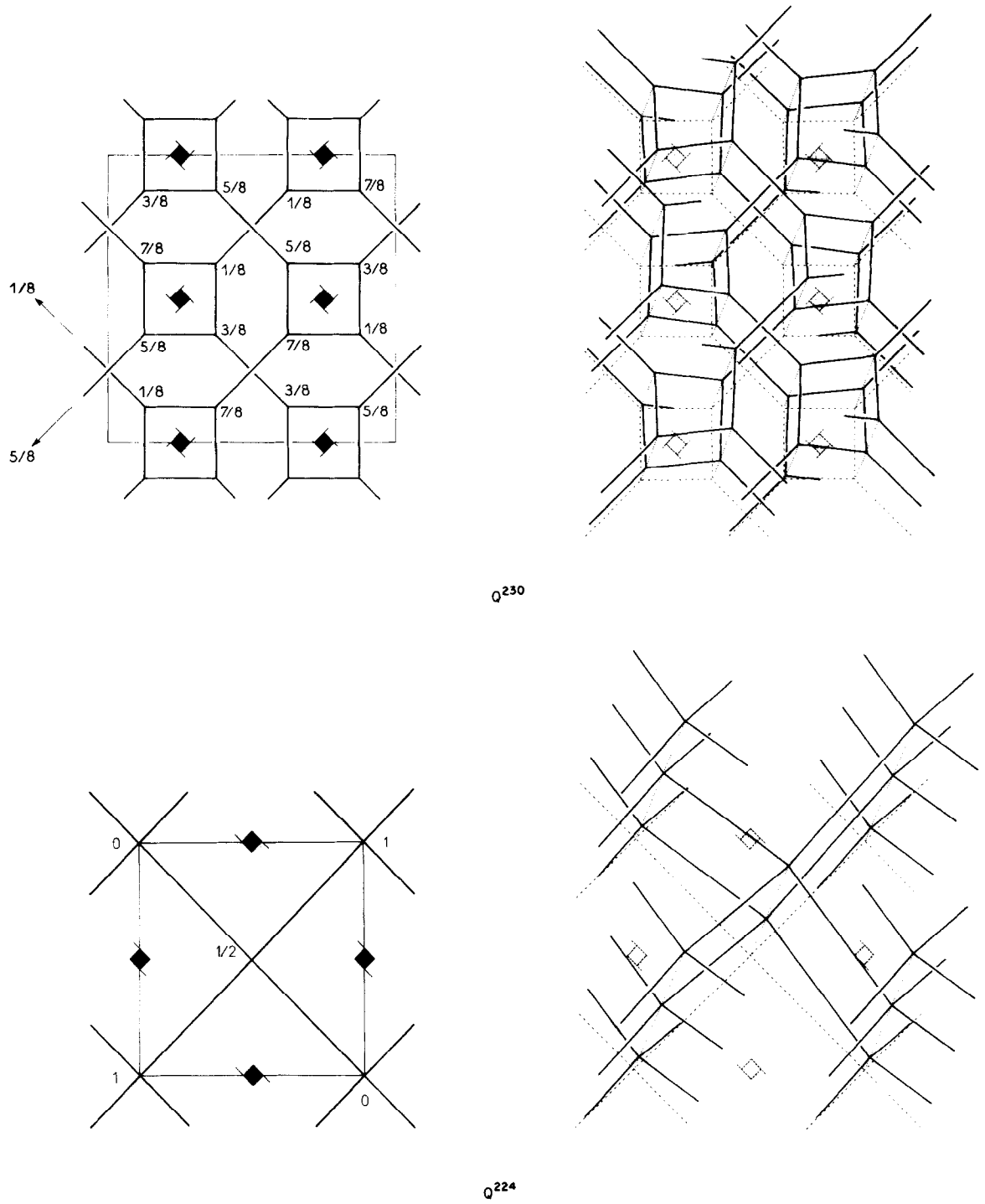

Figure 13. The structure of the cubic phases. The thick lines represent the axes of the rods. The 2 structures consist of 2 3-dimensional networks, intertwined and unconnected. Left frames: representation of the unit cell with the position of the rods and of the 4-fold axes. Right frames: perspective view of the structure. Upper frames: phase Q^{230}. Note that the rods are coplanarly joined 3 by 3. Lower frames: phase Q^{224}. Note that the rods are joined tetrahedrally 4 by 4. (See Appendix 2.)

identified five different cubic phases on the basis of an X-ray scattering study of a variety of lipids.

We observe here two phases of that type, which we label with the letter Q and the space group number (International Tables for X-ray Crystallography, 1952):

Q^{230}, space group $Ia3d$
Q^{224}, space group $Pn3m$.

Phase Q^{230} is characterized by a family of small-angle reflections whose reciprocal spacings ratios are $\sqrt{3} : \sqrt{4} : \sqrt{7} : \sqrt{8} : \sqrt{10} : \sqrt{11} : \ldots$. This phase is commonly observed in lipid–water systems; its structure was determined in 1967 and confirmed later (Luzzati & Spegt, 1967; Luzzati *et al.*, 1968*c*,1981).

Phase Q^{224} is characterized by the reciprocal

spacings ratios $\sqrt{2} : \sqrt{3} : \sqrt{4} : \sqrt{6} : \sqrt{8} : \sqrt{9} : \sqrt{10} : \ldots$. Tardieu (1972) observed this phase in phosphatidyl ethanolamine and proposed its structure (a brief description is also given by Tardieu & Luzzati, 1970). Longley & McIntosh (1983) observed this phase in glycerol mono-oleate and determined its structure, confirming Tardieu's proposal.

The structure of the two phases (see Fig. 13) consists of two three-dimensional networks of rods, mutually intertwined and unconnected. In Q^{230}, each junction involves three coplanar rods at an angle of 120°, and in Q^{224} four tetrahedrally oriented rods.

An interesting property of these structures (Luzzati *et al.*, 1968*c*) is the presence of two topologically distinct volumes, which can be visualized as the core of the rods and as the interstices between the rods, each continuous throughout the three-dimensional lattices and unconnected with the other. Structures of this type, but with smoother interfaces, are examples of infinite periodic minimal surfaces without intersections, discussed by Schwarz (1890) and Schoen (1970).

It is of some interest to determine a few geometric parameters of the two structures. We assume that the structures consist of identical straight rods of circular cross-section, whose ends are bevel-shaped to meet with two (Q^{230}) or three (Q^{224}) other rods. A simple geometric calculation shows that the volume ϕ and the surface area σ of each rod take the expressions:

$$\phi = \pi R^2 l(1 - k_v R/l), \tag{A7}$$

$$\sigma = 2\pi Rl(1 - k_s R/l). \tag{A8}$$

where l is the length of the rod, R is its radius, and k_v and k_s are constants whose values are tabulated below. The distance L_{max} from the furthest point to the surface of the rods and the shortest distance $2L_{min}$ between two unconnected rods can be determined also:

$$L_{max} = D_{max} - R. \tag{A9}$$

$$L_{min} = D_{min} - R. \tag{A10}$$

$$D_{max} = [(x_1 - x_2)^2 + (y_1 - y_2)^2 + (z_1 - z_2)^2]^{1/2}, \tag{A11}$$

$$D_{min} = ([(x_3 - x_4)^2 + (y_3 - y_4)^2 + (z_3 - z_4)^2]^{1/2})/2. \tag{A12}$$

The number n of rods in the unit cell of volume a^3, the length of each rod ($l = \lambda a$), the parameters k_v and k_s, the distances D_{max} and D_{min} and the coordinates of the points 1 to 4 of equations (A11) and (A12) are the following:

	n	λ	k_v	k_s	D_{max}/a	D_{min}/a
Q^{230}	24	$1/\sqrt{8}$	0·491	0·735	$\sqrt{5}/8$	$\sqrt{3}/8$
Q^{224}	4	$\sqrt{3}/2$	0·780	1·068	$1/\sqrt{8}$	$1/\sqrt{12}$

	1	2	3	4
Q^{230}	1/2, 1/2, 1/2	3/8, 1/2, 1/4	1/8, 1/8, 1/8	3/8, 3/8, 3/8
Q^{224}	1/2, 1/2, 0	1/3, 1/3, 1/3	3/4, 3/4, 1/4	1/4, 3/4, −1/4

Note also that the two structures are remarkably compact: the maximum volume fraction occupied by the rods, i.e. when their radius is equal to D_{min} (eqn (A10)), is 0·874 for Q^{230} and 0·927 for Q^{224}.

We are grateful to A. Gliozzi for bringing our two groups together, and to T. Gulik-Krzywicki, J. Seddon and A. Tardieu for a critical reading of the manuscript. We also thank A. Gliozzi and her co-workers for permission to quote their unpublished observations. This work was supported, in part, by grants from the Interface Physique-Biologie, Ministère de l'Industrie et de la Recherche and the Programma Finalizzato Chimica Fine e Secondaria, Comitato Nazionale delle Ricerche.

References

Brock, T. D. (1978). *Thermophilic Organisms and Life at High Temperatures*, Springer Verlag, New York, Heidelberg and Berlin.

Comita, P. B. & Gagosian, R. B. (1983). *Science*, **222**, 1329–1331.

de Kruijff, B., Cullis, P. R., Verkleij, A. J., Hope, M. J., Van Echteld, C. J. A. & Taraschi, T. F. (1984). In *Enzymes of Biological Membranes* (Martinosi, A., ed.), pp. 131–204, Plenum Press, New York.

De Rosa, M., Gambacorta, A. & Bu'lock, J. D. (1975). *J. Gen. Microbiol.* **86**, 136–164.

De Rosa, M., De Rosa, S., Gambacorta, A., Minale, L. & Bu'lock, J. D. (1977). *Phytochemistry*, **16**, 1961–1965.

De Rosa, M., De Rosa, S., Gambacorta, A. & Bu'lock, J. D. (1980*a*). *Phytochemistry*, **19**, 249–254.

De Rosa, M., Gambacorta, A., Nicolaus, B. & Bu'lock, J. D. (1980*b*). *Phytochemistry*, **19**, 821–825.

De Rosa, M., Esposito, E., Gambacorta, A., Nicolaus, B. & Bu'lock, J. D. (1980*c*). *Phytochemistry*, **19**, 827–831.

De Rosa, M., Gambacorta, A., Nicolaus, B., Ross, H. N. M., Grant, W. D. & Bu'lock, J. D. (1982). *J. Gen. Microbiol.* **128**, 343–348.

De Rosa, M., Gambacorta, A. & Nicolaus, B. (1983*a*). *J. Membr. Sci.* **16**, 287–294.

De Rosa, M., Gambacorta, A., Nicolaus, B. & Grant, W. D. (1983*b*). *J. Gen. Microbiol.* **129**, 2333–2337.

De Rosa, M., Gambacorta, A., Nicolaus, B., Chappe, B. & Albrecht, P. (1983*c*). *Biochim. Biophys. Acta*, **753**, 249–256.

Eriesson, B., Larsson, K. & Fontell, K. (1983). *Biochim. Biophys. Acta*, **729**, 23–27.

Fliermans, C. B. & Brock, T. D. (1972). *J. Bacteriol.* **111**, 343–350.

Gliozzi, A., Paoli, G., De Rosa, M. & Gambacorta, A. (1983). *Biophys. Biochim. Acta*, **735**, 234–242.

Gulik-Krzywicki, T., Rivas, E. & Luzzati, V. (1967). *J. Mol. Biol.* **27**, 303–322.

Huynh, S. (1973). *Biochimie*, **55**, 431–434.

International Tables for X-ray Crystallography (1952). The Kynoch Press, Birmingham, England.

Janiak, M. J., Small, D. M. & Shipley, G. G. (1976). *Biochemistry*, **21**, 4575–4580.

Kandler, O. (1982). *Archaebacteria*, Gustav Fisher Verlag, Stuttgart and New York.

Kates, M. & Kushwaha, S. C. (1978). In *Energetics and Structure of Halophilic Microorganisms* (Caplan, S. R. & Ginzburg, M., eds), pp. 461–479, Elsevier/North Holland Biomedical Press, Amsterdam.

Kushwaha, S. C., Kates, M., Juez, G., Rodríguez-Valera, F. & Kushner, D. J. (1982). *Biochim. Biophys. Acta*, **711**, 19–25.
Langworthy, T. A. (1977). *Biochim. Biophys. Acta*, **487**, 37–50.
Langworthy, T. A. (1982). *Curr. Topics Membr. Transport*, **17**, 45–77.
Larsson, K., (1983). *Nature (London)*, **304**, 664.
Longley, W. & McIntosh, T. J. (1983). *Nature (London)*, **303**, 612–614.
Luzzati, V. (1968). In *Biological Membranes*, (Chapman, D., ed.), vol. 1, pp. 71–123, Academic Press, London and New York.
Luzzati, V. (1981). *J. Physiol. (Paris)*, **77**, 1025–1028.
Luzzati, V. & Husson, F. (1962). *J. Cell Biol.* **12**, 207–219.
Luzzati, V. & Spegt, P. A. (1967). *Nature (London)*, **215**, 701–704.
Luzzati, V. & Tardieu, A. (1974). *Annu. Rev. Phys. Chem.* **25**, 79–92.
Luzzati, V., Reiss-Husson, F., Rivas, E. & Gulik-Krzywicki, T. (1966). *Ann. New York Acad. Sci.* **137**, 409–413.
Luzzati, V., Tardieu, A. & Gulik-Krzywicki, T. (1968*a*). *Nature (London)*, **217**, 1028–1030.
Luzzati, V., Gulik-Krzywicki, T. & Tardieu, A. (1968*b*). *Nature (London)*, **218**, 1031–1034.
Luzzati, V., Tardieu, A., Gulik-Krzywicki, T., Rivas, E. & Reiss-Husson, F. (1968*c*). *Nature (London)*, **220**, 485–488.
Luzzati, V., Tardieu, A. & Gulik-Krzywicki, T. (1981). *Proc. Nat. Acad. Sci., U.S.A.* **78**, 4683.
Rand, R. P. (1981). *Annu. Rev. Biophys. Bioeng.* **10**, 277–314.
Rand, R. P. & Luzzati, V. (1968). *Biophys. J.* **8**, 125–137.
Rivas, E. & Luzzati, V. (1969). *J. Mol. Biol.* **41**, 261–275.
Schoen, A. H. (1970). NASA Technical Note D-5541, Washington, DC.
Schwarz, H. A. (1890). *Gesammelte Mathematische Abhandlung*, **1**, Springer, Berlin.
Seddon, J. M., Cevc, G., Kaye, R. D. & Marsh, D. (1984). *Biochemistry*, **23**, 2634–2644.
Shipley, G. G. (1973). In *Biological Membranes*, (Chapman, D., ed.), vol. 2, pp. 1–89, Academic Press, London and New York.
Tardieu, A. (1972). Thesis, Université Paris Sud.
Tardieu, A. & Luzzati, V. (1970). *Biochim. Biophys. Acta*, **219**, 11–17.
Tardieu, A., Luzzati, V. & Reman, F. C. (1973). *J. Mol. Biol.* **75**, 711–733.
Tornabene, T. G., Langworthy, T. A., Holzer, G. & Oró, J. (1979). *J. Mol. Evol.* **13**, 73–83.
Woese, C. R. (1981). *Sci. Amer.* June 1981, 94–106.

Note added in proof. Our conclusion that the unsubstituted glycerols do not behave as ordinary polar headgroups is also consistent with the absence of liquid crystalline phases in diglycerides and with the recent report by Subipto Das & R. P. Rand (*Biochem. Biophys. Res. Commun.* (1984) **128**, 491–496) showing that small amounts of diacylglycerol have dramatic effects on the structure of lipid–water phases.

Edited by A. Klug